OPEN ACCESS
CellPress

Cell Reports
Report

Birthdate and Outgrowth Timing Predict Cellular Mechanisms of Axon Target Matching in the Developing Visual Pathway

Jessica A. Osterhout,[1] Rana N. El-Danaf,[1,2] Phong L. Nguyen,[1,2] and Andrew D. Huberman[1,2,3,*]
[1]Neurobiology Section, Division of Biology, University of California, San Diego, La Jolla, CA 92093, USA
[2]Neurosciences Department, University of California, San Diego, La Jolla, CA 92093, USA
[3]Department of Ophthalmology, University of California, San Diego, La Jolla, CA 92093, USA
*Correspondence: ahuberman@ucsd.edu
http://dx.doi.org/10.1016/j.celrep.2014.06.063

SUMMARY

How axons select their appropriate targets in the brain remains poorly understood. Here, we explore the cellular mechanisms of axon target matching in the developing visual system by comparing four transgenic mouse lines, each with a different population of genetically labeled retinal ganglion cells (RGCs) that connect to unique combinations of brain targets. We find that the time when an RGC axon arrives in the brain is correlated with its target selection strategy. Early-born, early-arriving RGC axons initially innervate multiple targets. Subsequently, most of those connections are removed. By contrast, later-born, later-arriving RGC axons are highly accurate in their initial target choices. These data reveal the diversity of cellular mechanisms that mammalian CNS axons use to pick their targets and highlight the key role of birthdate and outgrowth timing in influencing this precision. Timing-based mechanisms may underlie the assembly of the other sensory pathways and complex neural circuitry in the brain.

INTRODUCTION

Neurons carrying distinct categories of sensory information establish highly specific patterns of connections in the brain and thereby link information about the outside world to the appropriate perceptions and actions. The establishment of this connectivity involves many developmental processes, some of which have been intensely studied, such as synapse formation, axon guidance, topographic mapping, and laminar targeting (Dickson, 2002; McLaughlin and O'Leary, 2005; Luo and Flanagan, 2007; McAllister, 2007; Huberman et al., 2010). However, several crucial aspects of neural circuit assembly remain unresolved. An important example is axon target matching: the process by which an axon distinguishes among and innervates specific target structures (Figure S1A). Axon target matching has been explored in detail for invertebrates and within vertebrate spinal circuits (Goodman and Shatz, 1993; Clandinin and Zipursky, 2002; Dasen and Jessell, 2009), but the basic cellular mechanisms that ensure emergence of this feature in the mammalian brain remain poorly understood. Achieving a thorough understanding of the cellular mechanisms for axon target matching is a crucial first step toward establishing molecular models of this process.

Eye-to-brain connections are a potentially powerful model system for probing the mechanisms of axon target matching. They are comprised of retinal ganglion cell (RGC) axons that as a general group all have the same function: to convey visual information to the brain. However, RGCs are highly diverse; they include ~20 subtypes, each responding best to a specific feature in the visual world such as luminance, directional motion, or contrast and projecting that information to a stereotyped collection of target structures in the brain (Dhande and Huberman, 2014). Eye-to-brain connections thus raise the opportunity to explore the development of axon target matching in the context of a brain circuit whose function is known and that includes a variety of cell types, each of which connect to multiple long-range targets residing along the same growth trajectory.

Here, we asked how functionally distinct categories of RGCs find and connect to their targets during development using four transgenic mouse lines, each with GFP selectively expressed in one or two RGC subtypes distributed throughout the retina (Figures S1 and S2; Huberman et al., 2009; Osterhout et al., 2011, Rivlin-Etzion et al., 2011, Dhande et al., 2013). We find that different RGCs employ very different cellular strategies to achieve axon target wiring specificity. Moreover, we find that the mode by which an RGC achieves that specificity systematically varies according to its birthdate and timing of axon ingrowth. These results shed light on the cellular mechanisms used to establish parallel visual pathways and, in doing so, offer a general proposal for how timing of cell birth and axon growth could impact the assembly of complex neural circuits in the brain.

RESULTS

Cdh3-RGC Axons Innervate Their Correct Targets during the Late Embryonic Period

At maturity, Cdh3-RGC axons project mainly to non-image-forming visual targets (Osterhout et al., 2011; Figure S2). When

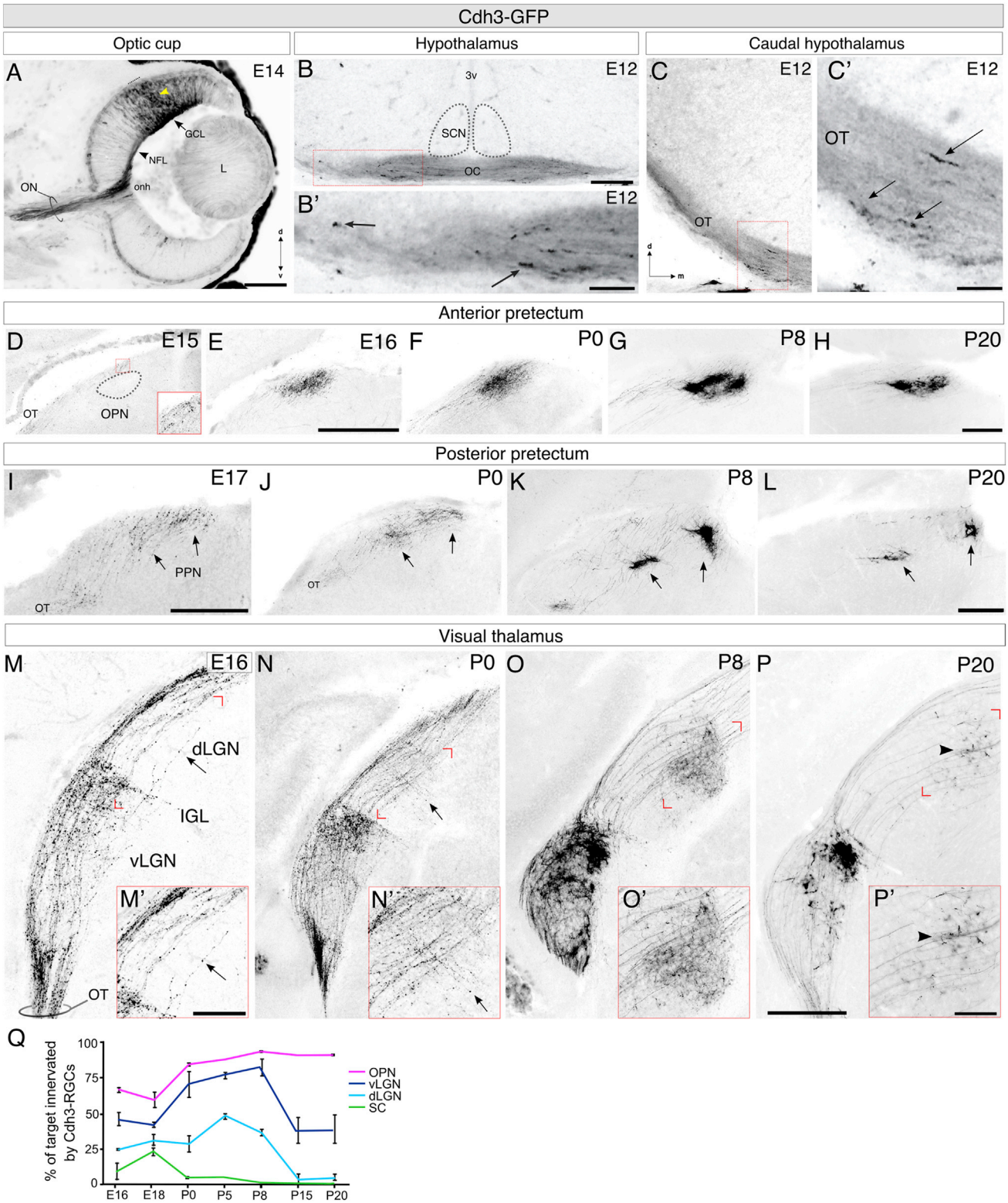

Figure 1. Cdh3-RGC Axons Innervate the Brain and Undergo Axon Target Matching during Late Embryogenesis

(A) Cdh3-RGCs migrating (yellow arrowhead) to the ganglion cell layer (GCL). Axons are entering the optic nerve head (onh) on E14. L, lens; ON, optic nerve; NFL, nerve fiber layer; d, dorsal; v, ventral. Scale bar represents 500 μm.

(legend continued on next page)

and how do Cdh3-RGCs find these targets? Cdh3-RGCs axons were visible in the eye and optic chiasm and optic tract by embryonic day 12 (E12; Figures 1A–1C′). On E15, Cdh3-RGC axons were observed in proximity to one of their future targets, the olivary pretectal nucleus (OPN; Figure 1D), but they were not observed within the OPN until E16 (Figure 1E). The density of Cdh3-RGC axons in the OPN increased from E16 to postnatal day 8 (P8; Figures 1E–1G), reaching maximum during the first postnatal week (Figure 1Q, magenta). From P8 to P20, Cdh3-RGC axons underwent slight refinement, such that their overall density of terminations was eventually reduced while the percent of overall target innervation remained unchanged (Figures 1G, 1H, and 1Q).

Cdh3-RGC axons were first detectable in their other major target, the posterior pretectal nucleus (PPN), by E17 (Figure 1I), where from P0 to P8, their terminals aggregated into two dense foci—a hallmark feature of retinal projections to this target (Figures 1J–1L; Osterhout et al., 2011). Together, these data reveal that Cdh3-RGCs begin to innervate their two main pretectal targets during late embryogenesis.

Target Selection by Cdh3-RGCs in the Developing Visual Thalamus

At maturity, Cdh3-RGCs project heavily to the thalamic intergeniculate leaflet (IGL) and ventral lateral geniculate nucleus (vLGN; Figures S2B and S2B′; Osterhout et al., 2011). Cdh3-RGCs innervate these nuclei by E16 (Figures 1M–1P). From E16 through the first postnatal week, Cdh3-RGCs also provided input to the dorsal lateral geniculate nucleus (dLGN; Figures 1M–1O), a target they project minimally to after P20 (Figures 1P, 1Q, and S2B; Osterhout et al., 2011). Interestingly, the route by which Cdh3-RGC axons reached the dLGN underwent dynamic shifts across development. At E16, Cdh3-RGC axons reached the dLGN by projecting dorsally, through the vLGN (Figures 1M and 1M′, arrow). By contrast, at P0, Cdh3-RGC axons sampled the dLGN via trajectories perpendicular to the optic tract (Figures 1N and 1N′, arrow), a configuration that closely resembles the target-entry routes of mature retino-dLGN axons (Dhande et al., 2011). By P8, Cdh3-RGCs also targeted the dorso-medial dLGN (Figures 1O and 1O′). Removal of Cdh3-RGC axons from the dLGN occurred gradually, occupying ~45% of the total target area on P8 and ~5% on P20 (Figure 1Q). Cdh3-RGC projections to the vLGN also diminished during this period (Figure 1Q). Thus, Cdh3-RGC axons select among several neighboring visual target structures in the thalamus by first sampling all of them and then by selectively removing inputs from just one of those targets, the dLGN.

Cdh3-RGCs Axons Initially Overshoot Their Future Targets

Notably, Cdh3-RGC axons grew beyond their future targets before innervating them. On E15, the axons of Cdh3-RGCs were seen in the optic tract, adjacent to the vLGN, IGL, and dLGN, but never *within* any of those targets (Figure 2A). At the same age, however, Cdh3-RGC axons were observed in the most distal visual target, the superior colliculus (SC; Figure 2B). Cdh3-RGC axons gradually increased in density within the SC until birth (Figures 2C, 2D, and 1Q), coinciding with innervation of thalamic and pretectal targets (Figure 1). They regressed from the SC after P0 such that by P20, only the occasional GFP-expressing axon was observed there (Figures 2D–2F and 1Q). Interestingly, the period when Cdh3-RGC axons were removed from the SC (P0–P20) coincided with the period when these axons increased in density within their more proximal targets, the OPN and PPN (Figure 1).

Removal of Cdh3-RGC Axons from the SC by Axon Retraction and Cell Death

To confirm the timing of Cdh3-RGC axon targeting, we carried out retrograde labeling (Figures 2G–2I). We injected cholera toxin β conjugated to Alexa Fluor 594 (CTβ-594) into the SC of P2 mice, then measured the percentage of CTβ+/Cdh3-GFP+ RGCs in the retina one day later on P3 (the "P2/3 group"; Figure 2J-L). We injected other mice on P19 and harvested their retinas on P20 (the "P19/20 group"; Figures 2M–2O). Approximately 29% of Cdh3-RGCs projected to the SC at P3 (Figures 2J–2L and 2S), whereas ~7% of Cdh3-RGCs projected to the SC at P20 (Figures 2M–2O and 2S). These values are generally consistent with our observations of Cdh3-RGC axons (Figures 2D and 2F).

To determine whether the removal of Cdh3-RGC axons from the SC reflects axon pruning, developmental cell death, or both, we injected the SC of P2 mice with CTβ-594 and waited until P20 to examine their retinas (the "P2/20 group"; Figures 2P–2R). By comparing the percentage of double-labeled CTβ+/Cdh3-GFP+ RGCs in the P2/3 versus P2/20 groups, we determined whether the RGCs that projected to the SC early in development remained viable. If both groups had the same percentage of double-labeled RGCs, we would conclude their axons retracted from the SC and either redirected or maintained

(B and B′) Cdh3-RGC axons at optic chiasm (OC) on E12. 3v, 3rd ventricle. Scale bar represents 250 μm. (B′) View of boxed region in (B); Cdh3-RGC axons (arrows). SCN, suprachiasmatic nucleus. Scale bars represent 250 μm.

(C and C′) Cdh3-RGC axons in optic tract (OT) on E12. (C′) Boxed region in (C). m, medial. Scale bar in (C′) represents 100 μm. Arrows, axonal profiles.

(D–H) Cdh3-RGC axons in the anterior pretectum on E15 (D), E16 (E), P0 (F), P8 (G), and P20 (H). OPN, olivary pretectal nucleus. Scale bars in (D)–(H) represent 250 μm. Scale bar in (E) is for (D) and (E). Scale bar in (H) is for (F)–(H).

(I–L) Cdh3-RGC axons in the posterior pretectum at E17 (I), P0 (J), P8 (K), and P20 (L). Arrows, posterior pretectal nucleus (PPN). Both scale bars represent 250 μm. Scale in (I) is for E17; scale in (L) is for (J)–(L).

(M–P) Cdh3-RGC axons in visual thalamus on E16 (M), P0 (N), P8 (O), and P20 (P). (M′–P′) High-magnification views. Arrow in (M and M′), Cdh3-RGC axons projecting through the vLGN to the dLGN. Scale bar in (M′) represents 100 μm. Arrow in (N and N′), Cdh3-RGCs send axons perpendicular from the OT into the dLGN. Arrowhead in (P and P′), a sparse group of Cdh3-RGC axon terminals found in the dLGN at P20. IGL, intergeniculate leaflet. Scale bar in (P) represents 200 μm for (M) and 300 μm for (N)–(P). Scale bar in (N′)–(P′) represents 100 μm.

(Q) Percentage of target containing GFP axons (%; ±SEM) in the OPN (magenta), vLGN (dark blue), dLGN (light blue), and superior colliculus (SC; green); n = 3–6 mice per age group.

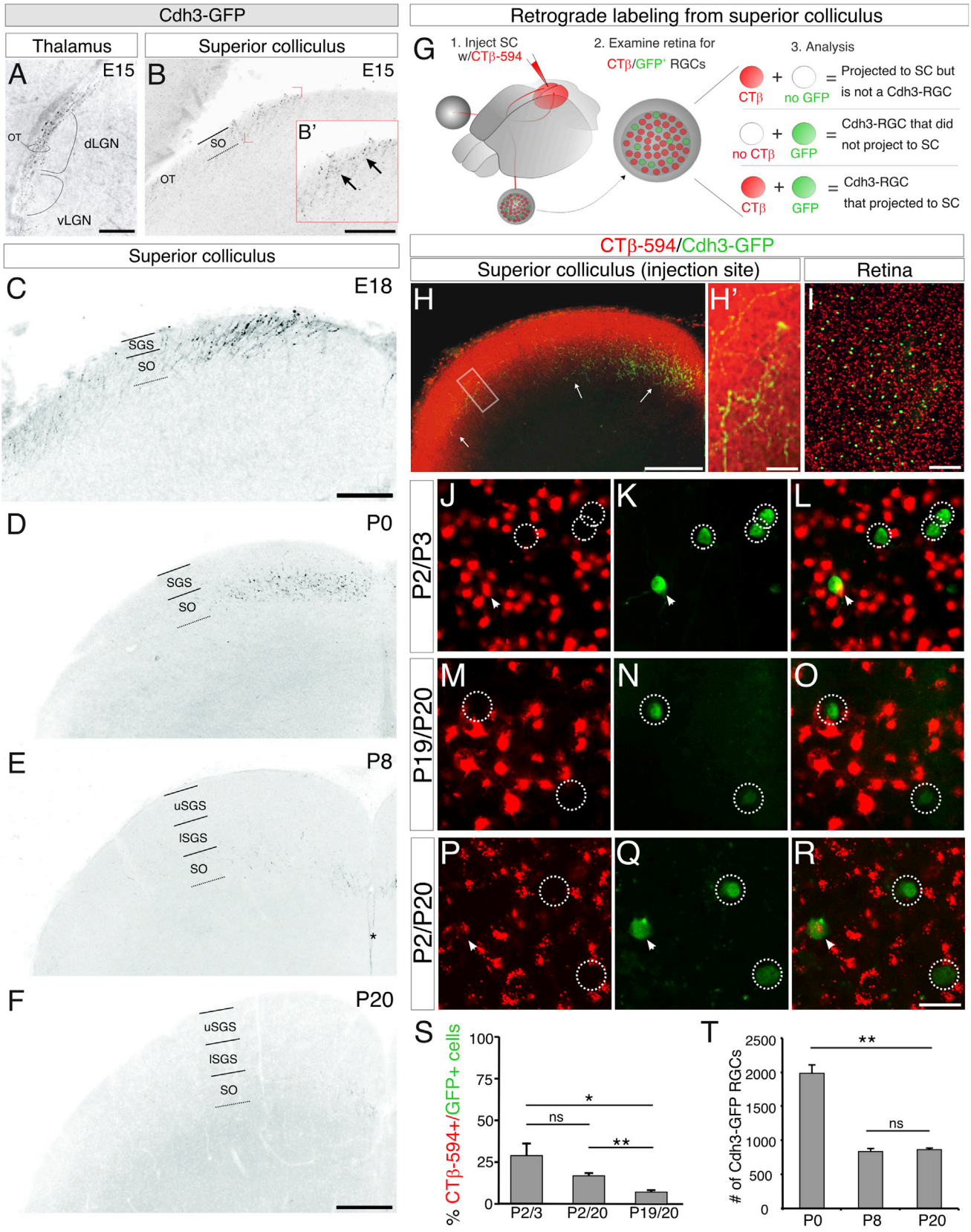

(legend on next page)

their inputs to more proximal targets (e.g., vLGN, OPN, or PPN). In P2/20 mice, ~17% of Cdh3-RGCs were double labeled (Figures 2P–2S), which is ~60% of the double-labeled cells observed in the P2/3 group. Thus, of the Cdh3-RGCs that projected to the SC on P2, some must have retracted their axons from the target and survived. However, because ~40% of Cdh3-RGCs that projected to the SC on P2 were gone by P20, they were likely removed by cell death, which occurs in the first postnatal week (O'Leary et al., 1986; Farah and Easter, 2005). Indeed, the number of GFP-expressing Cdh3-RGCs was reduced by approximately half from P0 to P8 but remained consistent from P8 to P20 (Figure 2T). We therefore conclude that Cdh3-RGCs removed their inputs to the SC through a combination of axon retraction and cell death.

Refinement of Cdh3-RGC Axons Is Unlikely to Reflect Dynamic Patterns of GFP Expression

The data presented thus far support the idea that Cdh3-RGCs undergo substantial overshoot and remodeling of their axon projections to achieve target specificity. To address if these changes simply reflect transient GFP expression, we analyzed which subtypes express Cdh3-GFP across development. We used three standard criteria for "typing" RGCs: dendritic morphology, dendritic lamination, and cell-type-specific markers. First, we targeted live Cdh3-RGCs in explants and filled them to reveal their dendritic branching (Figure S3A). The same two morphologically distinct RGC subtypes expressed GFP in both adult (P28–P94) and P8 Cdh3-GFP mice: Cdh3-subtype 1, which was studded with spiny protrusions on its proximal and distal dendrites (Figures S3B—S3C″), and Cdh3-subtype 2, which had a smaller dendritic tree with smooth proximal dendrites and fine-studded, distal dendrites (Figures S3D–S3E″; n = 9 cells per age).

We also examined the dendritic stratification patterns of the Cdh3-RGCs in the retinas of P3, P8, and P20 mice costained for vesicle acetylcholine transporter (VAChT), which labels S2 and S4, the "Off" and "On" sublayers in the inner plexiform layer (IPL), respectively. At all ages, we found two consistent RGC subtype-specific patterns of dendritic stratification. Cdh3-subtype 1 monostratified its dendrites vitreal to S4 (Figures S3F–S3H′), and Cdh3-subtype 2 bistratified its dendrites scleral to S2 and vitreal to S4 (Figures S3I–S3K′).

Next, we stained Cdh3-GFP retinas for molecular markers known to restrict their expression to specific RGC types. Because early in development Cdh3-RGCs project to the dLGN and the SC we used two markers (Cart and SMI32) that, at maturity, label the RGCs that stably project to those targets (Dhande et al., 2013; Kay et al., 2011). At P8 and P20, <6% of Cdh3-RGCs express Cart or SMI32 (Figures S3L–S3R). We also stained for melanopsin, which labels ~10% of adult Cdh3-RGCs (Osterhout et al., 2011). At P8, ~6% of Cdh3-RGCs expressed melanopsin, and this increased to ~11% by P20 (Figures S3L and S3S–S3X). The fact that the dendritic morphology, stratification, and molecular marker expression of Cdh3-RGCs is consistent from early postnatal development into adulthood argues that the changes in axon projection patterns we observed are unlikely to originate from shifting patterns of GFP expression but instead are likely to reflect reordering of axons projection patterns originating from the same two RGC subtypes across time.

Highly Precise Axon Target Matching by Hoxd10-RGCs to the Accessory Optic System Occurs Postnatally

Next, we explored the emergence of axon target matching for Hoxd10-RGCs, which, at maturity, project mainly to nuclei of the accessory optic system (AOS; Figures S1H–S1K and S2G–S2L′; Dhande et al., 2013). Hoxd10-RGC axons were first detectable in AOS targets, the medial terminal nucleus (MTN) and nucleus of the optic tract (NOT) at P7, their density increasing there from P8 to P15 (Figures 3A–3H). Hoxd10-RGC projections to their other targets, the dLGN and SC, also developed postnatally from P8 to P15 (Figures 3I–3N). Notably, we never observed Hoxd10-RGC axons innervating brain targets other than the ones they project to in the adult. Thus, Hoxd10-RGC axons arrive in the brain much later than Cdh3-RGC axons do and do not transiently sample any targets.

We considered the possibility that the apparent late arrival of Hoxd10-RGC axons reflected limited GFP expression at young ages. However, Hoxd10-RGCs expressed GFP as early as E16, and GFP+ somas were clearly visible throughout the ganglion cell layer of the retina starting at P0 (Figures S4F–S4J). We also used retrograde filling from the SC to address whether Hoxd10-RGCs project into the visual system at ages before P7. At P3, 19% of Hoxd10-RGCs projected to the SC

Figure 2. Early Ingrowth and Subsequent Removal of Cdh3-RGC Axons to the Superior Colliculus

(A and B) Cdh3-RGC axons growing past their future targets in the visual thalamus and into the caudal-most visual target, the superior colliculus (SC) on E15. (B) Cdh3-RGCs in the stratum opticum (SO) of the E15 SC. (B′) View of the framed region in (B); arrows, axons. Scale bar in (A) and (B) represents 250 μm.

(C–F) Cdh3-RGC axons in SC at E18 (C), P0 (D), P8 (E), and P20 (F). Scale in (C), 125 μm. Asterisk in (E), midline glia. SGS, stratum griseum superficialis; uSGS, upper; lSGS, lower tier (D–F). Scale bars represent 250 μm.

(G) Retrograde labeling.

(H) CTβ-594 injection into SC at P3. Retinorecipient layers are red, and Cdh3-RGC axons are green. Scale bar represents 250 μm.

(H′) Boxed region from (H). Scale bar represents 25 μm.

(I) CTβ-594 retrogradely labeled RGCs and Cdh3-RGCs. Scale bar represents 200 μm.

(J–L) CTβ-594 injected into SC on P2, retina harvested on P3; P2/3. (J) CTβ-594 backfilled RGCs, (K) Cdh3-GFP RGCs, (L) merged J and K.

(M–O) P19/20 Cdh3-GFP retina. CTβ-594 RGCs (M), Cdh3-RGCs (N), and merged (O).

(P–R) P2/20 Cdh3-GFP retina. (P) CTβ-594 RGCs, (Q) Cdh3-RGCs, (R) merge. Arrowhead, double-labeled cell. Circles, non-CTβ-594 Cdh3-GFP RGCs. Scale bar represents 100 μm.

(S) Percentage of total GFP-expressing RGCs that are also retrogradely labeled with CTβ-594 (±SEM). n = 2–3 mice per group; one-tailed t test, *$p < 0.05$, **$p < 0.01$.

(T) Number of Cdh3-RGCs at P0, P8, and P20 (n = 3 mice per age; **$p < 0.01$); ±SEM.

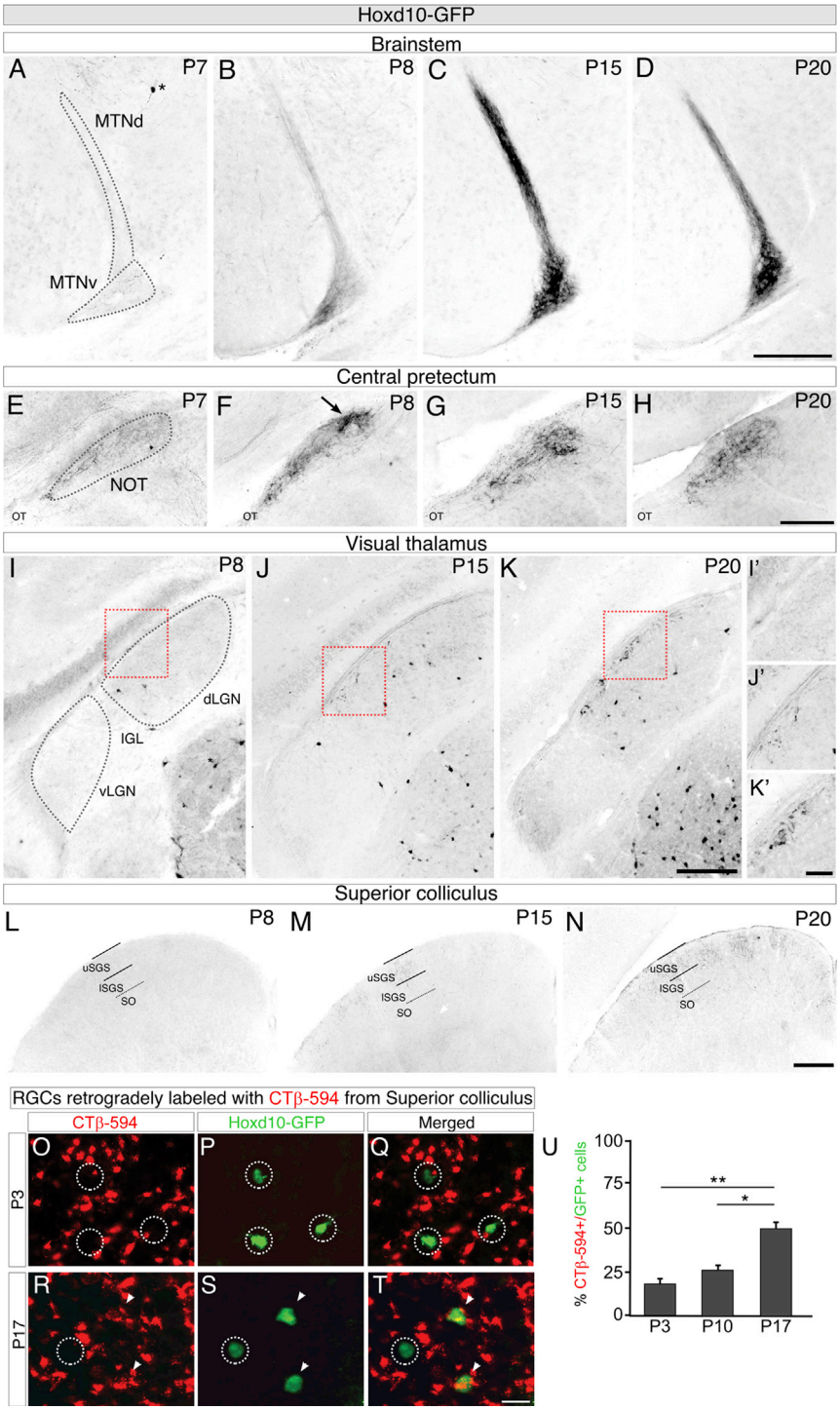

Figure 3. Axon Target Matching for Hoxd10-RGCs Begins Postnatally

(A–D) Hoxd10-RGC axons in the dorsal and ventral medial terminal nucleus (dMTN and vMTN) at P7 (A), P8 (B), P15 (C), and P20 (D). Asterisk, nonretinal GFP-expressing neuron. Scale bar represents 250 μm.

(E–H) Hoxd10-RGC axons in the nucleus of the optic tract (NOT) at P7 (E), P8 (F), P15 (G), and P20 (H). Arrow in (F), cluster of GFP expressing axons. Scale bar represents 250 μm.

(I–K′) Hoxd10-RGC axons in visual thalamus at P8 (I and I′), P15 (J and J′), and P20 (K and K′). Scale bar in (I)–(K) represents 250 μm. Scale bar in (I′)–(K′) represents 40 μm.

(L–N) Hoxd10-RGC axons in SC at P8 (L), P15 (M), and P20 (N). Scale bar represents 250 μm.

(O–Q) Hoxd10-GFP retinas retrogradely labeled with CTβ-594 (O) from the SC on P2 followed by harvest and analysis of Hoxd10-RGCs (P) on P3. Circles, Hoxd10-RGCs that do not contain CTβ-594. Scale bar represents 100 μm.

(R–T) CTβ-594 (R) after injection to the SC at P16 (harvest on P17). Hoxd10-RGCs (S); (T) merge. Circles, GFP+ RGC somas that lack CTβ-594. Arrowheads, double-labeled RGCs.

(U) Percentage of total GFP RGCs that are double-labeled (±SEM), n = 2 mice. *p < 0.05, **p < 0.01.

(Figures 3O–3Q and 3U). This value increased to 27% by P10 and to the mature value of 51% by P17 (Figures 3R–3U). Thus, direct visualization of Hoxd10-GFP axons and retrograde labeling both indicate the vast majority of Hoxd10-RGC axons innervate their targets during the second postnatal week.

The fact that Hoxd10-RGCs did not transiently sample any targets supports the idea that the same cohort of RGCs express GFP in both young and mature Hoxd10-GFP mice. Nonetheless, we characterized the dendritic morphology and stratification patterns of Hoxd10-RGCs at P5, P8, and adult. At all ages, we observed the same two GFP-expressing RGC subtypes: the dendrites of Hoxd10-subtype 1 stratified in the S4 sublaminae of the IPL and had swellings on their distal processes (Figures S5A–S5D′), and the dendrites of Hoxd10-subtype 2 stratified in S2 and S4 and had densely packed arbors tipped with end-terminal swellings (Figures S5E–S5H′; Dhande et al., 2013). Thus, throughout the axon targeting phase, the same two subtypes of RGCs express GFP in this mouse line.

DRD4-RGC Axons Innervate Their Brain Targets Postnatally and Make Minimal Errors

We then analyzed axon target matching for a third population of RGCs, DRD4-RGCs, which at maturity project to the dLGN and SC, but not to the pretectum or to accessory optic targets (Figures S1H–S1M and S2M–S2R′; Huberman et al., 2009; Kay et al., 2011). Although P0 DRD4-RGCs clearly expressed GFP (Figure S4L), very few DRD4-RGC axons were visible in the dLGN at that age (Figure 4A). Starting at P3, DRD4-RGC axons were visible in the optic tract and innervating the dLGN (Figure 4B). By P5, DRD4 axons were seen in the dLGN region adjacent to the optic tract

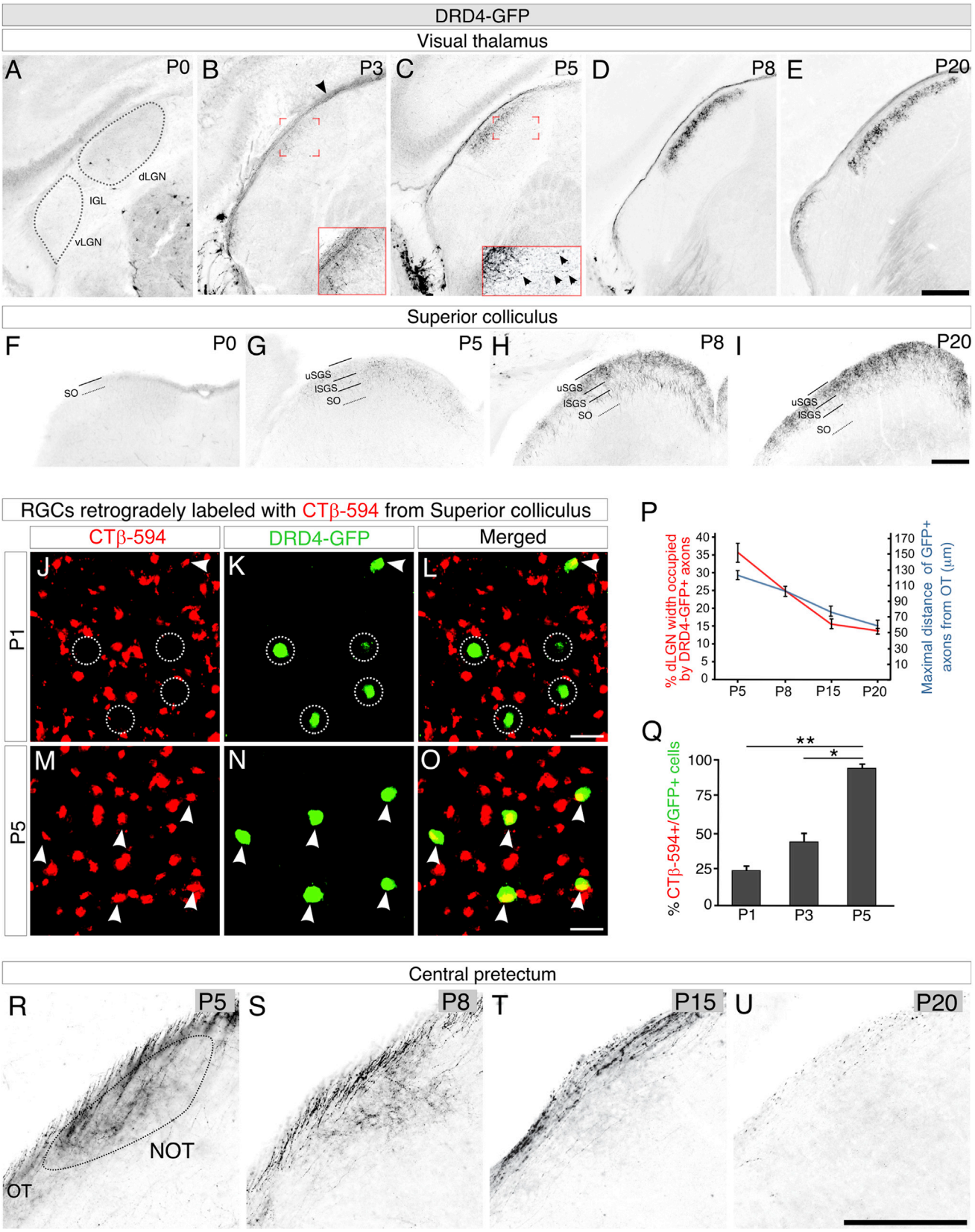

(legend on next page)

called the "shell" (Figure 4C; Krahe et al., 2011), their density increasing there from P5 to P20 (Figures 4C–4E and 4P). Interestingly, when they first arrived, some DRD4-RGC axons overshot the shell into the more medial dLGN and then refined to the correct zone (Figure 4C, inset, and quantified in Figure 4P).

DRD4-RGC projections to the SC followed a similar overall time course: their axons arrived from P0 to P5 (Figures 4F and 4G), filled the upper stratum griseum superficiale (uSGS) by P8, and appeared adult-like by P20 (Figure 4H, I). We confirmed this timeline by retrograde labeling and found that 23% of DRD4-RGCs projected to the SC on P1, ~42% on P3, and ~93% on P5 (Figures 4J–4O and 4Q). Thus, just like Hoxd10-RGC axons, DRD4-RGC axons innervate their targets postnatally.

DRD4-RGCs Transiently Project to the Accessory Optic System

In contrast to Hoxd10-RGCs, we found that DRD4-RGCs initially trespassed into an accessory optic target; they innervated the NOT and persisted there from P5 to P8 (Figures 4R and 4S), after which they exited this target between P15 and P20 (Figures 4T and 4U). Interestingly, the timing of DRD4-RGC axon removal from the NOT coincided with the stage when Hoxd10-RGC axons entered this target (Figure 3F), suggesting possible competition between axons arising from these two RGC populations (see discussion below).

To address the possibility that DRD4-RGC projections to the NOT resulted from transient expression of GFP in AOS-projecting RGC subtypes, we examined their morphologies and dendritic lamination patterns across development. At P8 and P20, DRD4-RGCs displayed the classically described dendritic characteristics of On-Off direction selective retinal ganglion cells (DSGCs): thick primary arbors and looping arborizations (Figures S5I–S5J″). In addition, the dendrites of P3 DRD4-RGCs bistratified and cofasciculated with the processes of starburst amacrine cells in S2 and S4 of the IPL, hallmark features of On-Off DSGCs (Figures S5K–S5P′; Huberman et al., 2009; Beier et al., 2013). At both P8 and P20, ~100% of DRD4-RGCs expressed the On-Off DSGC marker, Cart (Kay et al., 2011), and < 1% expressed the alpha RGC marker, SMI32 (Figures S5Q–S5Y). Thus, we conclude that transient DRD4-RGC axon projections we observed in the NOT arise from genuine mistargeting of these axons to the AOS rather than transient expression of GFP in other RGC subtypes.

Other Late-Arriving RGC Populations Are Also Highly Accurate in Their Targeting Choices

To further test whether the time of axon arrival relates to axon target matching strategy, we examined a fourth mouse line, TRHR-GFP, which labels On-Off DSGCs with distinct physiological characteristics and overall projection patterns from that of DRD4-RGCs, Cdh3-RGCs, or Hoxd10-RGCs (Figure S2; Rivlin-Etzion et al., 2011; Stafford et al., 2014). TRHR-RGCs arrived in the brain and innervated their targets predominantly during the second postnatal week (Figures 5C, 5G, and 5I). Few TRHR-RGC axons were visible in the dLGN or SC at P5 (Figures 5A and 5E) but from P8-P20 they filled the dLGN shell (Figures 5B–5D) and innervated the uSGS of the SC by P8 (Figures 5F–5H). TRHR-RGC axonal projections to the NOT followed a similar time course (Figure 5I). We did not observe evidence for TRHR-RGCs transiently innervating any targets (Figure 5I). Thus TRHR-RGCs, just like Hoxd10-RGCs, arrive in the brain relatively late and select their correct targets from the outset. When compared to each other, the four RGC populations examined here reveal a clear relationship between the time of axon arrival and the number of incorrect targets transiently innervated (Figure 5J).

Birthdates Vary across RGC Subtypes in a Manner that Correlates with Target Innervation Strategy

If the time when an RGC axon arrives in the visual pathway is an important determinant of the target-matching strategy it uses, then it is important to consider the factors that underlie that timing. One idea is timing of birth. In order to address whether the different RGC populations examined are born at different stages, we labeled terminally dividing cells with 5-ethynyl-2′-deoxyuridine (EdU) in Cdh3-, DRD4-, and Hoxd10-GFP mice during embryogenesis. We injected pregnant female mice with EdU at E10, E12, E14, or E16, harvested their offspring's retinas when they were P8, and quantified the number of EdU/GFP+ RGCs (Voinescu et al., 2009; McNeill et al., 2011). We discovered that each of the three RGC populations had unique birthdating profiles (Figures 5K–5U). Approximately 25% of Cdh3-RGCs were born at E10, and the number of newly born Cdh3-RGCs peaked at E12 (Figures 5K–5M and 5T). By contrast, only ~5% of DRD4-RGCs were born at E10, and the number of newly born EdU-labeled DRD4-RGCs peaked at E14 (Figures 5N–5P and 5T). The fraction of EdU-labeled Hoxd10-RGCs was also highest at E14, but a higher fraction of them were born at E16 relative to the other two RGC populations we examined (Figure 5T).

Figure 4. DRD4-RGCs Innervate Their Targets Postnatally and Transiently Innervate One Target

(A–E) DRD4-RGC axons in the dLGN at P0 (A), P3 (B), P5 (C), P8 (D), and P20 (E). Arrowhead in (B), GFP+ axons in the OT. Inset in (B), a few GFP labeled axons innervating the dLGN. Inset in (C), high magnification of DRD4-RGC axons extending past their appropriate layer (arrowheads). Quantified in (P). Scale bar represents 250 μm.

(F–I) DRD4-RGC axons in the SC at P0 (F), P5 (G), P8 (H), and P20 (I). Scale bar represents 250 μm.

(J–O) DRD4-RGCs retrogradely labeled from SC. Scale bar represents 100 μm. (J–L) CTβ-594 (J) injected on P0 and DRD4-RGCs (K) analyzed for double labeling at P1 (L).

(M–O) Retrograde CTβ-594 (M) labeled DRD4-RGCs (N), analyzed for double labeling (O) at P5; arrowheads, double-labeled cells; circles, nonretrogradely labeled DRD4-RGCs.

(P) Refinement of DRD4-RGCs axons in the dLGN at P5 (n = 5 mice), P8 (n = 5 mice), P15 (n = 5 mice), and P20 (n = 3 mice). Red line, percentage of total width of the dLGN occupied by DRD4-RGC axons. Blue line, maximum distance of DRD4-RGC axons from the OT (in μm). (±SEM).

(Q) Double-labeled DRD4-RGCs. n = 2 mice per age group.

(R–U) DRD4-RGC axons in the NOT at P5 (R), P8 (S), P15 (T), and P20 (U). Scale bar represents 250 μm.

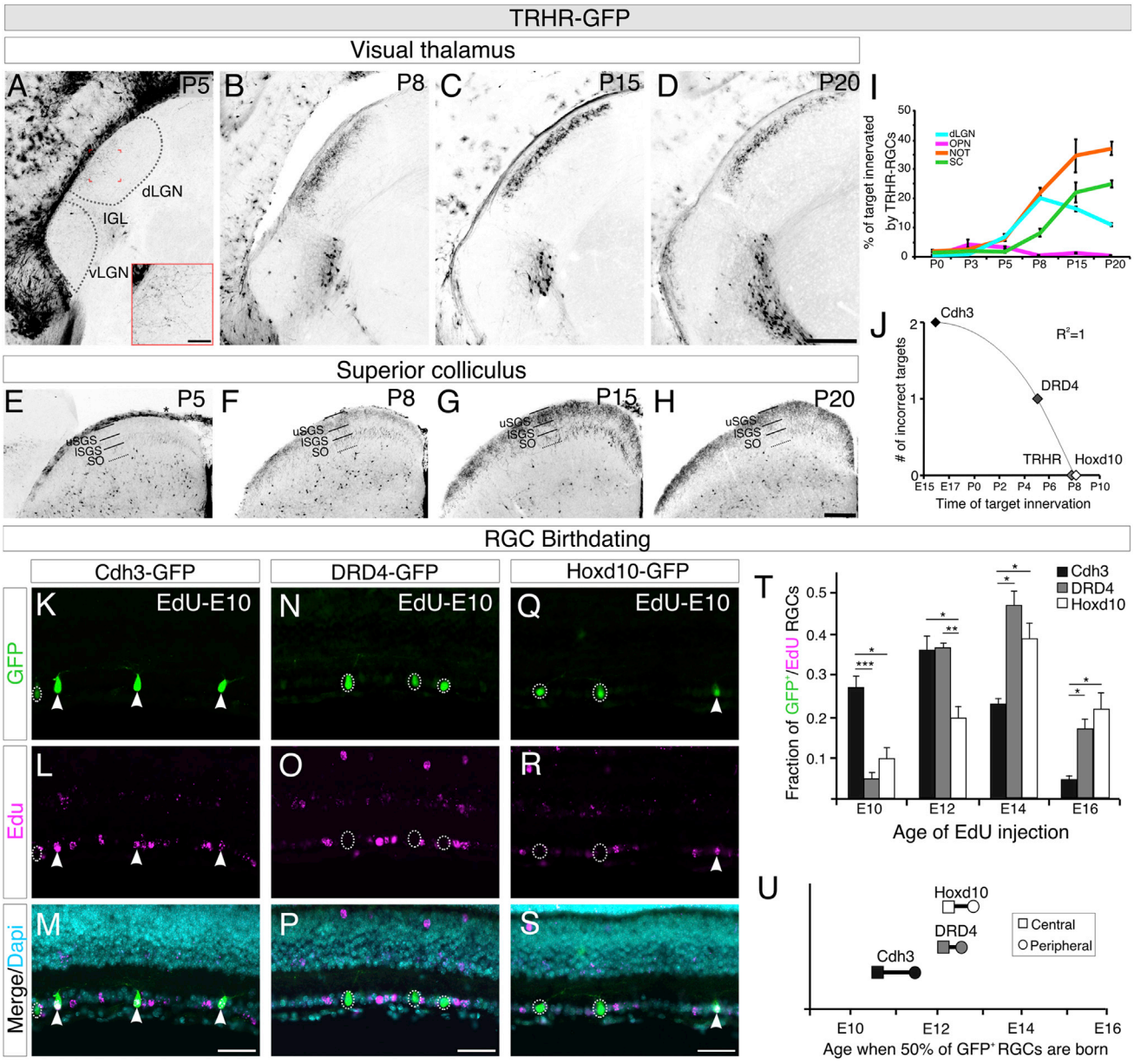

Figure 5. General Rules for Postnatal Axon Target Matching and Relationship to RGC Birthdate

(A–D) TRHR-RGC axons in dLGN at P5 (A), P8 (B), P15 (C), and P20 (D). Scale bar represents 250 μm. Boxed region in (A), scale bar represents 50 μm.

(E–H) TRHR-RGC axons in the SC at P5 (E; asterisk: GFP+ meninges), P8 (F), P15 (G), and P20 (H). Scale bar represents 250 μm.

(I) Quantification of TRHR-RGC axon projections to the dLGN (light blue), OPN (magenta), NOT (orange), and SC (green); n = 3–4 mice per age group; ±SEMs.

(J) Each RGC population examined here follows a general rule for axon target matching; time of target innervation correlates with the number of incorrect targets transiently innervated during development.

(K–S) Retinas from P8 mice injected with EdU at embryonic day 10 (E10): Cdh3-GFP mice (K–M), DRD4-GFP mice (N–P), Hoxd10-GFP mice (Q–S), GFP (top row), and EdU (middle row). Merge with DAPI (bottom row). Scale bar represents 50 μm.

(T) GFP-expressing RGCs labeled with EdU at a given age of injection; ±SEM.

(U) Age when 50% of the central (box) and peripheral (circle) GFP-expressing RGCs were born.

To account for any regional variations across the retina in RGC birthdating profiles, we also examined when 50% of EdU/GFP double-labeled RGCs were born in the central versus peripheral retina. Although there were slight differences according to retinal location (Figure 5U), this did not alter the overall relationship between RGC population and birthdate described above; neurogenesis of Cdh3-RGCs occurs relatively earlier than for other RGC populations. DRD4- and Hoxd10-RGCs were born at similar times, with Hoxd10-RGCs exhibiting a relatively protracted period of neurogenesis (Figures 5T and 5U). Along with

the findings above, these results indicate that RGC-category-specific birthdate correlates with when and how RGC axons select their targets.

DISCUSSION

Here, we explored how functionally distinct retinal neurons connect to their appropriate targets in the brain. Cellular explorations of other visual circuit assembly events have been instrumental in defining molecular models of those processes and indeed went on to become broadly influential. For example, models of retinotopic and eye-specific mapping emerged from the findings that RGCs initially overshoot their correct topographic and eye-specific zones before remapping to the appropriate locations, examples that thematically extend across many brain circuits (Shatz, 1996; McLaughlin and O'Leary, 2005; Feldheim and O'Leary, 2010).

Our first discovery is that different RGC populations employ different strategies to achieve accurate axon target matching. Cdh3-RGCs extended the entire length of the visual pathway before innervating intermediate targets. Subsequently, these axons refined their projections, stabilizing only those located in correct targets. The finding that RGCs sample different targets before refining their connections has precedence from classic studies in other species (Ramoa et al., 1989) but whether this was a general rule for all RGCs was not addressed. In fact, transient sampling of incorrect targets is not a general rule. The axons of Hoxd10-, DRD4-, and TRHR-RGCs were far more selective. DRD4-RGCs transiently sampled only one target (the NOT), and both Hoxd10- and TRHR-RGCs exhibited no transient targeting whatsoever.

Our second finding is that strategy of axon target matching is correlated with timing of axon growth. The axons of the three populations of RGCs that underwent minimal target sampling all arrived at their targets postnatally. By contrast, Cdh3-RGC axons reached the brain very early and underwent widespread refinement. Type 1 intrinsically photosensitive RGCs (M1 ipRGCs) also innervate their targets postnatally and do not make targeting errors (McNeill et al., 2011; Su et al., 2011). Thus, for five parallel eye-to-brain pathways, time of axon arrival correlates with the frequency of transient target innervation: early arrival correlates with extensive transient targeting, late arrival leads to no transient targeting, and axons that arrive in the interim transiently sample a minimal number of targets (Figure 5J).

Third, we found that RGC birthdates systematically relate to targeting strategy; early-born RGCs undergo extensive reordering of their initial targeting choices compared to later-born RGCs. The impact of birthdate on targeting strategy may ultimately relate to differences in axon growth rates. Although RGCs are born during a relatively narrow timeframe (Figure 5T), they innervate the brain across a relatively broad period spanning pre- and postnatal life. RGC axons are known to undergo a dramatic reduction in growth rate as they transition from embryonic to postnatal period (Goldberg et al., 2002). Given our observations that Cdh3-, Hoxd10-, and DRD4-RGCs exhibit different birthdate profiles, they likely possess different axon growth rates as well.

Similarities between Axon Target Matching, Retinotopic, and Eye-Specific Mapping

The overshoot and transient sampling of intermediate targets in Cdh3-RGCs is reminiscent of topographic mapping, whereby RGC axons initially extend across the full extent of the SC and then remove the overshooting portion of their axon, a process that involves axon-axon competition (McLaughlin and O'Leary, 2005; Feldheim and O'Leary, 2010). Axon target matching may also involve competition, with early-arriving RGCs limiting target vacancy and thereby preventing entrance of subsequent-arriving axons. An "early arrival" competition model has also been proposed to explain development of eye-specific layers (Shatz, 1996). Future studies involving selective deletion of early-arriving RGCs would help test whether competitive interactions indeed regulate axon target matching.

Molecular Mechanisms for Axon Target Matching

RGC axon target matching very likely relies on both repellants and attractants. All populations of RGCs we examined grew past the suprachiasmatic nucleus, suggesting this target harbors repellants for many non-M1 RGCs. Slit-robo-repellant interactions prevent mammalian RGCs from growing into the ventral diencephalon (Ringstedt et al., 2000); such repulsion may act at various locations and spatial scales to influence RGC axon target specificity. Adhesion also plays a role in axon target matching. Cadherin-6 (Cdh6) is expressed by Cdh3-RGCs and by their targets. In mice lacking Cdh6, Cdh3-RGCs incorrectly project beyond those targets (Osterhout et al., 2011). In addition, Reelin (which can regulate cadherin expression) is required for accurate ipRGC targeting in the thalamus (Franco et al., 2011; Su et al., 2011).

Varying Modes of Axon Target Matching and the Establishment of Polysynaptic Circuits

An important consideration is that cells within brain targets are undergoing maturation during the same stages when axons innervate them. Generally speaking, early-arriving axons may play an important role in the maturation of targets and/or prime growth pathways for the arrival of subsequent axons via expression of molecular signals. Indeed, Chen and coworkers described a critical role for early-arriving "pioneer" axons in targeting of subsequent-arriving axons to the zebrafish tectum (Pittman et al., 2008). Notably, the arrival of RGC axons in the dLGN regulates ingrowth timing of corticogeniculate afferents by influencing repellent expression (Brooks et al., 2013; Seabrook et al., 2013). Thus, whether or not an axon chooses to bypass, transiently innervate, or stably connect to a given target may instruct the maturation of that immediate target and its downstream targets that together comprise parallel pathways. In these ways, the variety of targeting strategies used by functionally distinct neurons such as those demonstrated here could have broad influence on the overall wiring specificity of circuits in the mammalian brain.

EXPERIMENTAL PROCEDURES

Animals

Cadherin-3-EGFP (Cdh3-GFP), homeobox D10 enhanced GFP (EGFP; Hoxd10-GFP), dopamine receptor D4-EGFP (DRD4-GFP), and thyrotropin-releasing hormone receptor-EGFP (TRHR-GFP) mice were obtained

from MMRRC (Huberman et al., 2009; Osterhout et al., 2011; Rivlin-Etzion et al., 2011; Dhande et al., 2013). All procedures were in accordance with institutionally approved protocols at the University of California, San Diego.

Tissue Processing

Tissue was immunostained to enhance the GFP signal (Huberman et al., 2008). Antibodies used were rabbit anti-GFP (1:1,000; Invitrogen), guinea pig anti-GFP (1:1,000; Synaptic Systems), guinea pig anti-VAChT (1:1,000; Millipore), rabbit anti-Cart (1:1,000; Phoenix), mouse anti-SMI32 (1:1,000, Invitrogen), and rabbit anti-melanopsin (1:1,000; Advanced Targeting Systems).

Anterograde and Retrograde Labeling of RGC Axons

Anterograde labeling with CTβ-594 was as described previously (Huberman et al., 2008). For retrograde labeling, a pulled-glass capillary pipette was used to inject through the skull; CTβ-594 (0.5–1.0 μl; at 0.5% in saline) was bilaterally pressure-injected into the SC.

Identifying Targets and Within-Target Locations for Analysis

Retinorecipient nuclei were identified by whole-eye labeling with CTβ-594 and target boundaries determined by landmarks and comparison to Godement et al. (1984). Images were acquired from the middle third of each target.

Quantification of Percentage of Target Area Occupied by GFP-Expressing Axons

Area fraction measurements were quantified in ImageJ. Mean pixel value of the background was measured in a 250 μm × 250 μm area devoid of GFP labeling and then used to subtract background signal. The "area fraction" tool was used to find the percent of target occupied by GFP+ axons. Measurements were taken from three to eight tissue sections in each target, depending on target size and age.

Quantification of Within-dLGN Refinement

Maximum distance occupied by axons across the lateral-medial extent of the dLGN taken with the "line measurement" tool in ImageJ. Three measurements per tissue section (dorsal, middle, and ventral) and three tissue sections per animal (rostral, middle, and caudal) were analyzed, for a total of nine measurements per mouse (n = 5 mice per age group).

RGC Marker Analysis

Retinas from three mice were analyzed. Approximately 100 GFP+ RGCs, from multiple 250 μm × 250 μm regions at varying distances from the optic nerve head, were analyzed.

Targeted RGC Injections/Filling

Targeted fills were carried out as described previously (Beier et al., 2013).

Birthdating RGCs

Pregnant females were injected with EdU (20 μg/g body weight; Invitrogen). The Click-iT EdU Alexa Fluor Imaging kit (Invitrogen) was used to detect EdU before primary antibody staining. EdU-labeled RGCs were quantified from eight to ten retinal sections (n = 3). A cumulative fraction graph using a two-degree polynomial curve was used to calculate the day at which 50% of cells were born in the central and peripheral retina ($R^2 > 0.98$ for all curves; Voinescu et al., 2009).

SUPPLEMENTAL INFORMATION

Supplemental Information includes five figures and can be found with this article online at http://dx.doi.org/10.1016/j.celrep.2014.06.063.

AUTHOR CONTRIBUTIONS

J.A.O. and A.D.H. conceived the experiments, J.A.O. and P.L.N. performed histology, J.A.O. imaged and analyzed all data, R.N.E.-D. did the RGC filling, and J.A.O. and A.D.H. wrote the paper.

ACKNOWLEDGMENTS

We thank Drs. Tina Schwabe, Tom Clandinin, and Tania Seabrook for helpful comments and Pritha P. Multani for help with histology. Supported by NIH RO1 EY022157-01 (A.D.H.), the E. Matilda Ziegler Foundation (A.D.H), a Pew Scholar Award (A.D.H.), and a National Science Foundation Graduate Research Fellowship under grant DGE-1144086 (J.A.O.).

Received: September 5, 2013
Revised: April 25, 2014
Accepted: June 30, 2014
Published: July 31, 2014

REFERENCES

Beier, K.T., Borghuis, B.G., El-Danaf, R.N., Huberman, A.D., Demb, J.B., and Cepko, C.L. (2013). Transsynaptic tracing with vesicular stomatitis virus reveals novel retinal circuitry. J. Neurosci. *33*, 35–51.

Brooks, J.M., Su, J., Levy, C., Wang, J.S., Seabrook, T.A., Guido, W., and Fox, M.A. (2013). A molecular mechanism regulating the timing of corticogeniculate innervation. Cell Reports *5*, 573–581.

Clandinin, T.R., and Zipursky, S.L. (2002). Making connections in the fly visual system. Neuron *35*, 827–841.

Dasen, J.S., and Jessell, T.M. (2009). Hox networks and the origins of motor neuron diversity. Curr. Top. Dev. Biol. *88*, 169–200.

Dhande, O.S., and Huberman, A.D. (2014). Retinal ganglion cell maps in the brain: implications for visual processing. Curr. Opin. Neurobiol. *24*, 133–142.

Dhande, O.S., Hua, E.W., Guh, E., Yeh, J., Bhatt, S., Zhang, Y., Ruthazer, E.S., Feller, M.B., and Crair, M.C. (2011). Development of single retinofugal axon arbors in normal and β2 knock-out mice. J. Neurosci. *31*, 3384–3399.

Dhande, O.S., Estevez, M.E., Quattrochi, L.E., El-Danaf, R.N., Nguyen, P.L., Berson, D.M., and Huberman, A.D. (2013). Genetic dissection of retinal inputs to brainstem nuclei controlling image stabilization. J. Neurosci. *33*, 17797–17813.

Dickson, B.J. (2002). Molecular mechanisms of axon guidance. Science *298*, 1959–1964.

Farah, M.H., and Easter, S.S., Jr. (2005). Cell birth and death in the mouse retinal ganglion cell layer. J. Comp. Neurol. *489*, 120–134.

Feldheim, D.A., and O'Leary, D.D. (2010). Visual map development: bidirectional signaling, bifunctional guidance molecules, and competition. Cold Spring Harb. Perspect. Biol. *2*, a001768.

Franco, S.J., Martinez-Garay, I., Gil-Sanz, C., Harkins-Perry, S.R., and Müller, U. (2011). Reelin regulates cadherin function via Dab1/Rap1 to control neuronal migration and lamination in the neocortex. Neuron *69*, 482–497.

Godement, P., Salaün, J., and Imbert, M. (1984). Prenatal and postnatal development of retinogeniculate and retinocollicular projections in the mouse. J. Comp. Neurol. *230*, 552–575.

Goldberg, J.L., Klassen, M.P., Hua, Y., and Barres, B.A. (2002). Amacrine-signaled loss of intrinsic axon growth ability by retinal ganglion cells. Science *296*, 1860–1864.

Goodman, C.S., and Shatz, C.J. (1993). Developmental mechanisms that generate precise patterns of neuronal connectivity. Cell Suppl. *72*, 77–98.

Huberman, A.D., Manu, M., Koch, S.M., Susman, M.W., Lutz, A.B., Ullian, E.M., Baccus, S.A., and Barres, B.A. (2008). Architecture and activity-mediated refinement of axonal projections from a mosaic of genetically identified retinal ganglion cells. Neuron *59*, 425–438.

Huberman, A.D., Wei, W., Elstrott, J., Stafford, B.K., Feller, M.B., and Barres, B.A. (2009). Genetic identification of an On-Off direction-selective retinal ganglion cell subtype reveals a layer-specific subcortical map of posterior motion. Neuron *62*, 327–334.

Huberman, A.D., Clandinin, T.R., and Baier, H. (2010). Molecular and cellular mechanisms of lamina-specific axon targeting. Cold Spring Harb. Perspect. Biol. *2*, a001743.

Kay, J.N., De la Huerta, I., Kim, I.J., Zhang, Y., Yamagata, M., Chu, M.W., Meister, M., and Sanes, J.R. (2011). Retinal ganglion cells with distinct directional preferences differ in molecular identity, structure, and central projections. J. Neurosci. *31*, 7753–7762.

Krahe, T.E., El-Danaf, R.N., Dilger, E.K., Henderson, S.C., and Guido, W. (2011). Morphologically distinct classes of relay cells exhibit regional preferences in the dorsal lateral geniculate nucleus of the mouse. J. Neurosci. *31*, 17437–17448.

Luo, L., and Flanagan, J.G. (2007). Development of continuous and discrete neural maps. Neuron *56*, 284–300.

McAllister, A.K. (2007). Dynamic aspects of CNS synapse formation. Annu. Rev. Neurosci. *30*, 425–450.

McLaughlin, T., and O'Leary, D.D. (2005). Molecular gradients and development of retinotopic maps. Annu. Rev. Neurosci. *28*, 327–355.

McNeill, D.S., Sheely, C.J., Ecker, J.L., Badea, T.C., Morhardt, D., Guido, W., and Hattar, S. (2011). Development of melanopsin-based irradiance detecting circuitry. Neural Dev. *6*, 8.

O'Leary, D.D., Fawcett, J.W., and Cowan, W.M. (1986). Topographic targeting errors in the retinocollicular projection and their elimination by selective ganglion cell death. J. Neurosci. *6*, 3692–3705.

Osterhout, J.A., Josten, N., Yamada, J., Pan, F., Wu, S.W., Nguyen, P.L., Panagiotakos, G., Inoue, Y.U., Egusa, S.F., Volgyi, B., et al. (2011). Cadherin-6 mediates axon-target matching in a non-image-forming visual circuit. Neuron *71*, 632–639.

Pittman, A.J., Law, M.Y., and Chien, C.B. (2008). Pathfinding in a large vertebrate axon tract: isotypic interactions guide retinotectal axons at multiple choice points. Development *135*, 2865–2871.

Ramoa, A.S., Campbell, G., and Shatz, C.J. (1989). Retinal ganglion beta cells project transiently to the superior colliculus during development. Proc. Natl. Acad. Sci. USA *86*, 2061–2065.

Ringstedt, T., Braisted, J.E., Brose, K., Kidd, T., Goodman, C., Tessier-Lavigne, M., and O'Leary, D.D. (2000). Slit inhibition of retinal axon growth and its role in retinal axon pathfinding and innervation patterns in the diencephalon. J. Neurosci. *20*, 4983–4991.

Rivlin-Etzion, M., Zhou, K., Wei, W., Elstrott, J., Nguyen, P.L., Barres, B.A., Huberman, A.D., and Feller, M.B. (2011). Transgenic mice reveal unexpected diversity of on-off direction-selective retinal ganglion cell subtypes and brain structures involved in motion processing. J. Neurosci. *31*, 8760–8769.

Seabrook, T.A., El-Danaf, R.N., Krahe, T.E., Fox, M.A., and Guido, W. (2013). Retinal input regulates the timing of corticogeniculate innervation. J. Neurosci. *33*, 10085–10097.

Shatz, C.J. (1996). Emergence of order in visual system development. Proc. Natl. Acad. Sci. USA *93*, 602–608.

Stafford, B.K., Park, S.J., Wong, K.Y., and Demb, J.B. (2014). Developmental changes in NMDA receptor subunit composition at ON and OFF bipolar cell synapses onto direction-selective retinal ganglion cells. J. Neurosci. *34*, 1942–1948.

Su, J., Haner, C.V., Imbery, T.E., Brooks, J.M., Morhardt, D.R., Gorse, K., Guido, W., and Fox, M.A. (2011). Reelin is required for class-specific retinogeniculate targeting. J. Neurosci. *31*, 575–586.

Voinescu, P.E., Kay, J.N., and Sanes, J.R. (2009). Birthdays of retinal amacrine cell subtypes are systematically related to their molecular identity and soma position. J. Comp. Neurol. *517*, 737–750.